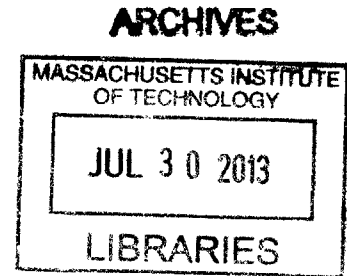A Contrast Agent for MRI of Calcifications in Breast Cancer

by

Jonathan Marmurek

BESc, Electrical Engineering
MESc, Biomedical Engineering
The University of Western Ontario

Submitted to the Harvard-MIT Division of Health Sciences and Technology
in Partial Fulfillment of the Requirements of the Degree of

Master of Science in Health Sciences and Technology

at the

MASSACHUSETTS INSTITUTE OF TECHNOLOGY

June 2013

Signature of Author ....
Harvard-MIT Division of Health Sciences and Technology
May 20, 2013

Certified by ....
Robert E. Lenkinski, PhD
Distinguished Professorship in Medical Science, UT Southwestern
Thesis Supervisor

Certified by ....
Bruce R. Rosen, MD, PhD
Professor in Radiology, Harvard Medical School
Thesis Co-Supervisor

Accepted by ....
Emery N. Brown, MD, PhD
Director, Harvard-MIT Program in Health Sciences and Technology
Professor of Computational Neuroscience and Health Sciences and Technology

A Contrast Agent for MRI of Calcifications in Breast Cancer

by

Jonathan Marmurek

Submitted to the Harvard-MIT Division of Health Sciences and Technology
on May 20, 2013 in Partial Fulfillment of the
Requirements for the Degree of Master of Science in
Health Sciences and Technology

ABSTRACT

Clinical x-ray mammography cannot delineate between hydroxyapatite and calcium oxalate, the respective forms of calcification in malignant and benign breast tumors. The water-poor nature of solid calcifications makes them difficult to image by conventional MRI. Recently, ultra-short echo time (UTE) MRI has enabled detection of solid calcified structures, but it is not specific to the underlying chemical composition. This thesis presents a hydroxyapatite-targeted gadolinium contrast agent for UTE MRI of calcification in malignant breast cancer.

The hydroxyapatite-targeted contrast agent was synthesized by conjugating a bisphosphonate, pamidronate, to a gadolinium chelate. Binding specificity was tested by UTE MRI of the contrast agent reacted with hydroxyapatite, calcium oxalate, and other calcium-based crystals. The sensitivity of the contrast agent for hydroxyapatite was evaluated by UTE MRI: the lowest detectable concentration of hydroxyapatite-adsorbed contrast was 1 µM. Longitudinal relaxation time measurements were used to estimate the apparent relaxivity of the hydroxyapatite contrast agent to be >1000 s-1/mM. The targeted agent relaxivity is enhanced more than a 100-fold compared to conventional untargeted gadolinium contrast agents due to the restricted rotational motion of the contrast agent upon binding to a solid surface.

In-vivo MRI of systemic delivery of the contrast agent was demonstrated in an animal model for breast cancer with hydroxyapatite calcifications. Pre- and post-contrast UTE MRI were acquired with systemic contrast agent injections. Dual-echo UTE subtraction images between short and long echoes showed specific uptake of the contrast agent to the calcifications. The mean signal intensity of the calcified regions enhanced by 200% between pre- and post-contrast images, posing the hydroxyapatite-targeted contrast agent as a clinical diagnostic for distinguishing benign and malignant calcification forms in breast cancer.

Thesis Supervisor: Robert E. Lenkinski, PhD
Title: Distinguished Professorship in Medical Science, UT Southwestern

Thesis Co-supervisor: Bruce R. Rosen, MD, PhD
Title: Professor of Radiology, Harvard Medical School

Acknowledgements

I would like to thank all of those who supported me during my graduate studies at MIT. My supervisor, Dr. Robert Lenkinski, gave me the opportunity to contribute to this exciting project. Dr. Bruce Rosen's co-supervision was consistently practical and assuring. I am also grateful for my academic advisors, Drs. Martha Gray and Elfar Adalsteinsson, who were guiding sources throughout my coursework and research.

In addition to the overarching impact that these advisors had, there were many other people who contributed to my experience on a daily basis. Dr. Khaled Nasr trained me in organic synthesis and chemical validation, and was the chemist who designed the synthesis for the contrast agent developed in this thesis. Drs. Elena Vinogradov and Ananth Madhuranthakam helped me get started with the ultra-short echo time MRI sequence that I used throughout this research. Dr. Fangbing Liu provided the animal model, and Elaine Lunsford dedicated herself to helping with animal care, contrast agent injections, and CT imaging.

I could not ask for a better place to work than the close-knit MRI Research group at the Beth Israel Deaconess Medical Center. Together, the clinical researchers, MR technologists, post-doctoral fellows, and principal investigators, all have admirable expertise for me to draw upon when needed. I would especially like to thank Dr. David Alsop for keeping me welcome in the group.

Finally, my close friends, family, and parents were the backbone of my livelihood. Their undying encouragement is a large part of where I am today, and where I will be in the future.

Table of Contents

1.1. Breast cancer calcifications
1.2. MRI of breast cancer
1.3. Ultra-short echo time MRI
1.4. Contrast agent relaxivity
1.5. Proposal: A contrast agent for MRI of hydroxyapatite calcification in breast cancer

2.1. Methods and materials
    2.1.1. Targeting ligand synthesis
    2.1.2. Contrast agent synthesis
    2.1.3. Sample preparation
    2.1.4. Magnetic resonance imaging
    2.1.5. Data analysis – specificity, sensitivity, and relaxivity
2.2. Results
    2.2.1. Targeting specificity
    2.2.2. Sensitivity
    2.2.3. Free and bound agent relaxivity
2.3. Discussion

3.1. Methods and materials
    3.1.1. Systemic uptake to slurry implants
        3.1.1.1. Slurry implantation
        3.1.1.2. Pre- and post-contrast imaging
        3.1.1.3. CT validation
        3.1.1.4. Image analysis
    3.1.2. Systemic uptake to hydroxyapatite calcification in a breast cancer model
        3.1.2.1. Breast cancer microcalcification model
        3.1.2.2. Pre- and post-contrast imaging
        3.1.2.3. Image analysis
    3.1.3. Statistics

3.2. Results
    3.2.1. Hydroxyapatite and calcium oxalate slurry imaging
    3.2.2. MRI of hydroxyapatite calcification in breast tumors
3.3. Discussion

4.1. Major contributions and impact
4.2. Limitation and pitfalls
4.3. Future work and recommendations

List of Figures and Tables

Chapter 1. Introduction

1.1. Breast cancer calcifications

Breast cancer is the most prevalent form of cancer in women [1]. Every year in the United States, there are over 200,000 newly diagnosed cases and over 30,000 deaths from the disease. The American Cancer Society recommends that women over the age of 40 receive annual screening exams [2] because earlier diagnosis provides improved outcomes. Detection of solid microcalcifications by x-ray mammography is the primary clinical imaging finding in breast cancer tumors [3]. Type I microcalcifications are formed of calcium oxalate (CO) and occur only in benign tumors [4], whereas Type II microcalcifications are formed of hydroxyapatite (HA) and are more prevalent in malignant tumors [5,6]. While HA microcalcifications are a hallmark of malignant breast cancer, the chemical composition of microcalcifications cannot be determined by x-ray mammography. Currently, patterns in calcification size, shape, and localization are used to distinguish between benign and malignant tumors, and pathological assessment by biopsy confirms diagnosis of suspicious findings [7]. However, there are many forms of calcification in benign breast pathologies that are mistaken as suspicious. X-ray mammography has a high specificity but low sensitivity for detecting breast cancer [8], leading to a high number of unnecessary biopsies.

1.2. MRI of breast cancer

Women at higher risk of breast cancer, from family history or genetic predisposition (testing positive for the BRCA1/2 gene mutations), are recommended to receive annual screening starting at the age of 30 [8]. MRI screening is recommended in high-risk women because it has been shown to improve the detection of breast cancer when used in addition to x-ray

mammography. Some breast cancers which do not appear on x-ray are diagnosed by dynamic contrast enhanced (DCE) MRI [9,10,11]. The current DCE MRI screening protocol [12] uses a vascular non-targeted gadolinium contrast agent. MRI of the breast is collected pre- and post-contrast injections to look for regions of enhanced signal intensity caused by blood flow to a tumor. The time course for contrast agent uptake to the tumor is tracked following administration by plotting the tumor signal intensity over time. Different contrast uptake and washout patterns are representative of malignant, benign, and borderline tumors. While MRI improves the detection and treatment outcomes in high-risk women [13], some breast cancers remain undetected by combined x-ray/MRI screening.

1.3. Ultra-short echo time MRI

Solid calcified structures are low in water content and have very short transverse relaxation times (T_2 < 1 ms), making them difficult to detect by conventional MRI. The development of ultra-short echo time (UTE) imaging sequences has recently enabled the detection of short-T_2 calcifications in plaques [14], bone and connective tissue [15]. These UTE sequences use echo times from 10-1000 microseconds by shortening the acquisition with half excitation pulses and radial sampling of the free induction decay. While x-ray is very good at detecting solid calcifications, it is unable to differentiate the chemical composition of Type I (calcium oxalate) and Type II calcifications (hydroxyapatite) in benign and malignant tumors respectively. DCE-MRI currently used for breast cancer screening cannot detect calcifications at all. UTE MRI of breast cancer could enable the detection of calcifications, but would still not reveal their chemical composition. Combining UTE with a longitudinal relaxation gadolinium (Gd) contrast

agent that specifically targets hydroxyapatite would enable the detection and differentiation of the calcification forms in malignant breast cancer.

1.4. Contrast agent relaxivity

Gadolinium contrast agents alter the signal in MRI by shortening the longitudinal relaxation times (T_1) of surrounding protons. The change in relaxation rate for a local concentration of contrast agent is relaxivity: the characteristic measure relating the agent's sensitivity. The longitudinal relaxivity of conventional non-targeted paramagnetic contrast agents, described by the classical theory of Solomon, Bloembergen, and Morgan (SBM) [16,17,18], is affected primarily by the exchange rate of coordinated water molecules, the relaxation rate of paramagnetic electron spins, and the rotational correlation time of the molecule. The latter is the time in which a freely rotating paramagnetic ion in solution reorients. Slowly rotating molecules with long rotational correlation times are predicted to have high relaxivities [19,20], and previous work [21] has demonstrated that shorter linkers between a Gd-chelate and targeting-ligand reduce rotational freedom when bound. However, SBM theory requires random isotropic motion of a paramagnetic ion in solution whereas contrast agents bound to a surface are motion restricted. Contrast agents that are targeted to select surfaces may have restricted motions resulting in enhanced relaxivities optimal for imaging biological markers.

1.5. Proposal: A contrast agent for MRI of hydroxyapatite calcification in breast cancer

This thesis proposes a hydroxyapatite-targeted gadolinium contrast agent for UTE MRI of calcifications in malignant breast cancer. Pamidronate, a bisphosphonate known to bind hydroxyapatite with high affinity [22,23] will be conjugated by a short linker to a gadolinium

9

chelate. The specificity, sensitivity, and relaxivity of the contrast agent will be characterized *in-vitro*, and UTE MRI will be used to demonstrate *in-vivo* uptake to hydroxyapatite calcifications in animal models of breast cancer. The contrast agent has the potential to improve clinical breast cancer screening by MRI. UTE detection of the hydroxyapatite targeted contrast agent may help diagnose cancers missed by x-ray mammography and DCE MRI. Specification of the calcification type during screening may reduce unnecessary biopsies and lead to earlier detection and treatment of malignant breast cancer.

Chapter 2. *In-vitro* contrast agent development

This chapter presents the development of a targeted gadolinium contrast agent for MRI of

hydroxyapatite calcifications. The hydroxyapatite-targeted contrast agent is synthesized by

conjugating a bisphosphonate targeting ligand, pamidronate, to a gadolinium chelate. The

synthesis and *in-vitro* experiments testing specificity, sensitivity, and relaxivity are detailed.

The specificity of the contrast agent is evaluated by UTE MRI of the contrast agent reacted with

hydroxyapatite and calcium oxalate, the malignant and benign forms of calcification in breast

cancer, along with other varied calcium salts. The sensitivity, sought as the minimum detectable

dose concentration of hydroxyapatite-targeted contrast agent, is determined by imaging

incremental concentrations of contrast agent with hydroxyapatite. Lastly, longitudinal relaxation

times (T1) for increasing contrast agent concentrations are measured by UTE to estimate the

bound and free contrast agent relaxivities.

2.1. Methods and materials

2.1.1. Targeting ligand synthesis

The hydroxyapatite-targeting ligand, pamidronate, was synthesized according to Figure 2.1

based on reported routines [24]. Methyl groups protecting the bisphosphonate were required to

avoid chelation of gadolinium in the contrast agent synthesis. All chemicals were purchased from

Fischer Scientific (Pittsburgh, PA), Sigma-Aldrich (Saint Louis, MO), Macrocyclics (Dallas,

TX), VWR International (West Chester, PA), and Bachem (Torrance, CA), and were used as

received. The molecular weight of the synthesized reaction products were verified [25] by

analytical liquid chromatography and mass spectroscopy (LC-MS) using HPLC grade solvents
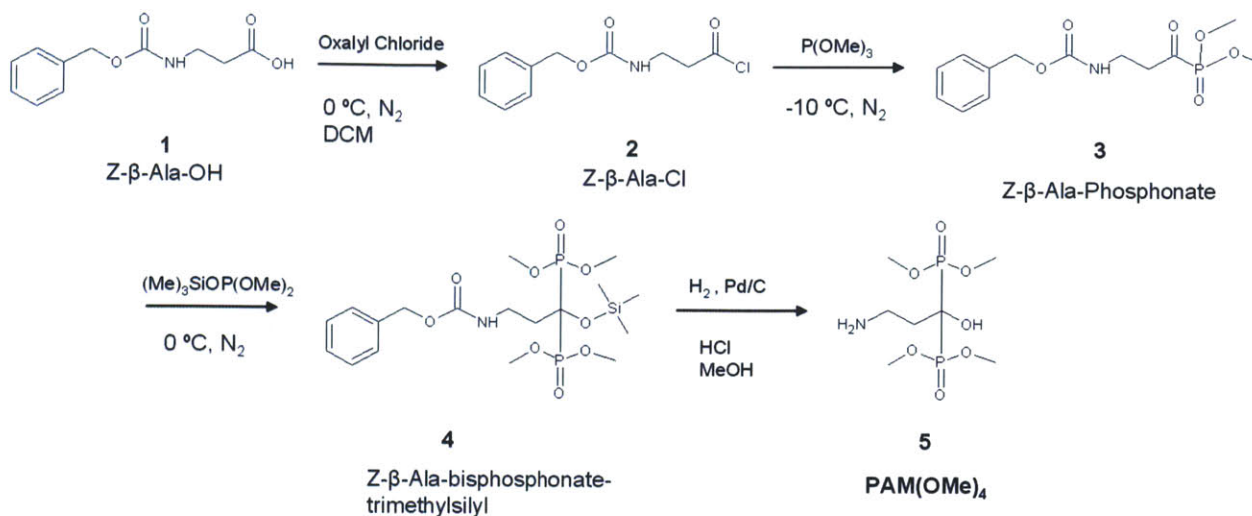
(Appendix 1).

Figure 2.1 – Synthesis of the pamidronate targeting ligand

Synthesis of *(2) Z-β-Ala-Cl*: 20 mmol (4.46 g) of *Z-β-Ala-OH* was dissolved in 40 mL anhydrous dichloromethane (DCM) and was reacted with oxalyl chloride (2 mL, 1.1 eq + excess) at 0 °C under nitrogen atmosphere overnight. The reaction mixture turned from cloudy white with precipitate flakes to a clear solution. Excess oxalyl chloride was removed by repeated (x5) rotary evaporation in DCM. The clear oily product, *Z-β-Ala-Cl*, was dried under vacuum for two hours (4.53 g, 94% yield).

Synthesis of *(3) Z-β-Ala-Phosphonate*: Trimethyl phosphate (3.0 mL, 20 mmol + excess) was added dropwise to the *Z-β-Ala-Cl* under nitrogen while stirring at -10 °C in an acetone/ice bath. The reaction reached room temperature and was stirred overnight. The crude product was washed by repeated addition, stirring, and decanting of hexanes. *Z-β-Ala-Phosphonate*, a slightly yellow oil, was dried under vacuum for two hours (5.67 g, 90% yield).

Synthesis of *(4) Z-β-Ala-bisphosphonate-trimethylsilyl*: Dimethyl trimethylsilyl phosphate (4.0 mL, 20 mmol + excess) was added to (3) while stirring under nitrogen atmosphere at 0 °C. The

mixture was reacted overnight at room temperature and the product, *Z-β-Ala-bisphosphonate-trimethylsilyl*, was washed repeatedly in hexanes and dried under vacuum (7.45 g, 75% yield).

Synthesis of *(5) PAM(OMe)₄*: The resultant Z-β-Ala-bisphosphonate-trimethylsilyl was dissolved in 60 mL methanol and 500 µL of hydrochloric acid was added. Following the addition of palladium catalyst (10% product by weight + excess) the compound underwent hydrogenolysis by shaking overnight under hydrogen atmosphere. The catalyst was filtered, and the solvent was removed by rotary evaporation. *PAM(OMe)₄* was isolated by dissolving the crude product in 2 mL ethyl acetate, and adding excess ether to crystallize the product into a flaky light-yellow solid. Excess solvent was decanted, and the *PAM(OMe)₄* (4.07 g, 70% yield) was dried under vacuum for further conjugation to a gadolinium-chelate contrast agent.

2.1.2. Contrast agent synthesis

The contrast agent, *Gd-DOTA-Ser-PAM* (GDSP) was synthesized according to Figure 2.2. The bisphosphonate targeting ligand, pamidronate, was conjugated to a Gd-DOTA chelate via a short Serine linker. The targeted contrast agent was synthesized by: forming a linker-ligand complex, conjugating the linker-ligand to DOTA, chelating gadolinium, and deprotecting the targeting ligand. The contrast agent preparation was modeled after existing ligand-agent conjugations strategies [26,27,28]. Characterization of the synthesized products was performed by liquid chromatography and mass spectroscopy (Appendix 1).

Synthesis of *(7) Z-Ser-(tBu)-PAM(OMe)₄*: *PAM(OMe)₄* (0.5 mmol) was dissolved in 20 mL of dichloromethane (DCM) and stirred for 30 minutes while the coupling agent O-Benzotriazole-N,N,N',N'-tetramethyl-uronium-hexafluoro-phosphate (HBTU, 1.1 eq.) and organic base N,N-Diisopropylethylamine (DIEA, 2.2 eq.) were added to *(6) Z-Ser-(tBu)-OH* (0.5 mmol) dissolved
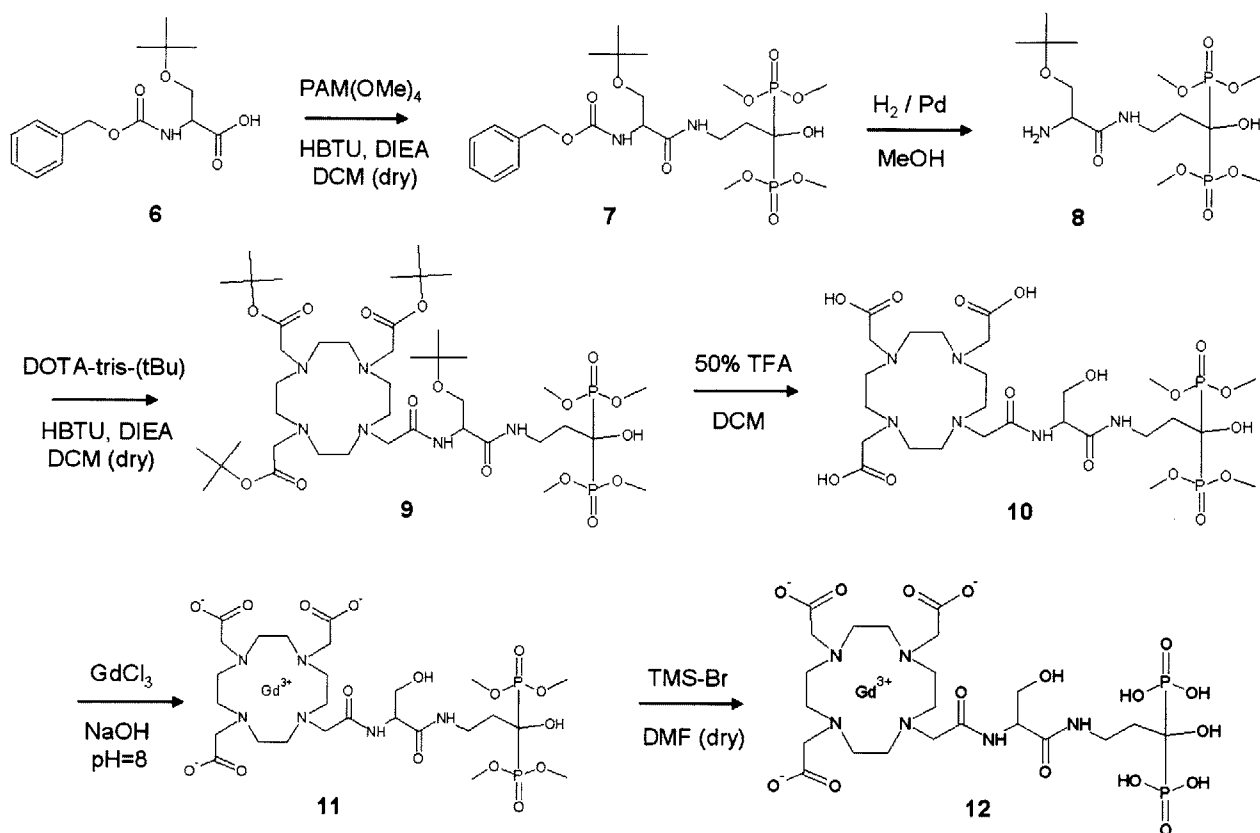
Figure 2.2 – Synthesis of the contrast agent Gd-DOTA-Ser-PAM

in 4 mL DCM , and then vortexed. The linker-coupling mixture was added to the *PAM(OMe)₄*

and was stirred overnight at room temperature. The reaction mixture was purified by liquid-

phase extraction in a separation funnel by washing with 10% (wt.) citric acid, saturated sodium

carbonate solution, and saturated sodium chloride solution. The organic layer, reserved through

the washings, was dried over sodium sulfate for 30 minutes and filtered before removing the

solvent by rotary evaporation. The clear oily product was dried under vacuum (216 mg, 76%

yield).

Synthesis of *(8) Ser-(tBu)-PAM(OMe)₄*: *Z-Ser-(tBu)-PAM(OMe)₄* (0.38 mmol) was dissolved in

40 mL of methanol and palladium catalyst was added (10% wt.). Hydrogenolysis proceeded

overnight by shaking the reaction vessel under hydrogen gas. The catalyst was filtered, the solvent was evaporated, and the linker-ligand product was dried under vacuum to a slightly yellow tinted oil (141 mg, 65% yield).

Synthesis of *(9) DOTA-tris-(tBu)-Ser-(tBu)-PAM(OMe)₄*: DOTA-tris-(tBu) (0.33 mmol) was dissolved in DCM (4 mL), HBTU (1.1 eq) and DIEA (2.2 eq) were added, and the mixture was vortexed for 30 minutes. The *Ser-(tBu)-PAM(OMe)₄* was dissolved in 20 mL DCM, the DOTA mixture was added, and the reaction was stirred overnight at room temperature. The clear oily product was isolated by extracting (in citric acid, sodium carbonate, and sodium chloride washes), drying the organic layer over sodium sulfate, filtering the solution, evaporating the solvent, and drying under vacuum (282 mg, 57 % yield).

Synthesis of *(10) DOTA-Ser-PAM(OMe)₄*: The DOTA-tris-(tBu)-Ser-(tBu)-PAM(OMe)₄ was dissolved in 4 mL DCM, and 4 mL of trifluroacetic acid (TFA) was added to deprotect the carboxylic acids. The reaction was stirred overnight at room temperature. After removing the solvent by rotary evaporation, the crude product was dissolved in 2 mL of methanol and was precipitated by adding 150 mL of ether. Excess TFA was removed by repeated washing in ether, and the white-powdered product was dried under vacuum (210 mg, 55% yield).

Synthesis of *(11) Gd-DOTA-Ser-PAM(OMe)₄*: Gadolinium chloride (0.30 mmol) was added to the *DOTA-Ser-PAM(OMe)₄* dissolved in distilled water (2 mL). The pH was adjusted to 8 by dropwise addition of NaOH, and the chelation reaction was stirred overnight at room temperature. The penultimate product was frozen in liquid nitrogen and lyophilized as a white powder (216 mg, 47% yield).

Synthesis of *(12) Gd-DOTA-Ser-PAM*: The *Gd-DOTA-Ser-PAM(OMe)₄* was dissolved in anhydrous N-N-dimethylformamide (1 mL) and was equilibrated to 0 °C under nitrogen atmosphere. Bromotrimethysilyl (8 eq.) was added and the mixture was reacted by stirring overnight. Water and methanol (20 mL each) were added to the crude product before evaporating solvent and lyophilizing to a yellowish crust. The product was isolated by dissolving in methanol (2 mL), precipitating in ether (100 mL), and washing with acetonitrile. The final product was dried under vacuum as a white powder (194 mg, 45% yield).

2.1.3. Sample preparation

To test the relative binding specificity of the contrast agent 10 µM GDSP in 1 mL water was reacted (1 hr, room temperature) with 25 mg each of hydroxyapatite (HA), calcium oxalate (CO), calcium carbonate (CC), calcium pyrophosphate (CPP), and calcium phosphate (CP). The reaction mixtures were washed by repeated vortexing, centrifugation, decanting and re-solvation to remove unbound contrast agent. The same five calcium salts in 1 mL water with no contrast agent, and reacted with 10 µM of non-targeted Gd-DOTA (Magnevist) in 1 mL water were used as controls. To test the sensitivity of GDSP adsorption to HA, increasing concentrations (0, 0.1, 1, 5, 10, 20, 50, 100, and 200 µM) of GDSP in 1 mL water were each reacted with 25 mg HA (1 hr, room temperature), and washed as above. The same concentrations of GDSP in water alone (with no crystals) were prepared to characterize the free contrast agent relaxivity. All crystal samples were prepared for imaging by centrifuging the pellets in 500 µL of water.

2.1.4. Magnetic resonance imaging

MR imaging was performed on a 1.5 T whole-body scanner (GE Healthcare, Sigma 15.0) using a custom-built birdcage transmit/receive coil. UTE images were acquired (slice thickness = 5 mm,

FOV = 9 cm, matrix = 256×199, NEX = 2, α = 90°, TE = 100 μs) at varied TR (50, 100, 200,

500, 2000, and 5000 ms) to measure the T_1 of the targeted and free GDSP samples. Comparative

images acquired using a standard fast gradient-echo (FGRE) sequence (slice thickness = 5 mm,

FOV = 9 cm, matrix = 256×256, NEX = 1, α = 30°, TE = 2.1 ms, varied TR) were used to

demonstrate the necessity of UTE imaging for detecting hydroxyapatite-bound contrast agent

under short T_2 conditions. Specificity was tested by imaging the 10 μM GDSP reacted with the

varied calcium salts, the crystals alone (with no contrast agent), and the crystals reacted with

non-targeted Gd-DOTA. The sensitivity limit was evaluated by imaging increasing

concentrations of HA-targeted GDSP over varied TR. The relaxivities of both the HA-targeted

and free GDSP were estimated from UTE T_1 measurements.

2.1.5. Data analysis – specificity, sensitivity, and relaxivity

The relative specificity of the contrast agent was assessed by comparing the mean ROI signal

intensities of each the control crystal types to the 10 μM GDSP-reacted crystals and to the

crystals reacted with non-targeted contrast agent. The ratio of percent change in mean ROI signal

intensity, with and without contrast agent, was used to calculate the relative specificity for

hydroxyapatite over other calcium salts as:

$$Specificity = \frac{(\overline{SI}_{HA}^{GDSP} - \overline{SI}_{HA}^{0})/\overline{SI}_{HA}^{0}}{(\overline{SI}_{i}^{GDSP} - \overline{SI}_{i}^{0})/\overline{SI}_{i}^{0}} \qquad \text{[Eqn. 2.1]}$$

where $\overline{SI}_{HA/i}^{GDSP/0}$ are the mean ROI signal intensities of the control crystals (0) and those reacted

with contrast agent (GDSP), for hydroxyapatite (HA) and the varied salts i = CO, CC, CPP, and

CP. The sensitivity of GDSP adsorption to HA was assessed from the UTE signal intensities as

the lowest detectable GDSP reaction concentration.

Longitudinal relaxation times (T_1) were estimated (ImageJ, MATLAB) by least-squares fitting of

the mean signal intensities of crystal ROIs, over varied repetition time (TR), to the signal

equation:

$$S_z(t) = S_0(1 - e^{-t/T_1})$$ [Eqn. 2.2]

where $S_z(t)$ is the longitudinal signal intensity, S_0 is the signal intensity at equilibrium (fully

relaxed), and t is the TR at which the measurement was taken. The apparent relaxivity (relating

change in relaxation rate to dose concentration) of the bound contrast was estimated at the

minimum detectable concentration as:

$$r_1^b = \Delta R_1/[\text{GDSP}]$$ [Eqn. 2.3]

where $R_1 = 1/T_1$, $\Delta R_1 = R_1^b - R_1^0$, R_1^b is the relaxation rate of the agent-bound HA crystals, R_1^0 is

the relaxation rate of the HA crystals alone, and [GDSP] is the initial dose concentration of the

contrast agent. The T_1 of increasing concentrations of free contrast agent were used to estimate

the free (unbound) GDSP relaxivity, r_1^u, by linear regression of:

$$R_1 = R_1^w + r_1^u [\text{GDSP}]$$ [Eqn. 2.4]

where R_1^w is relaxation time of water.

2.2. Results

2.2.1. Targeting specificity

The UTE MR images (TR = 100 ms, TE = 100 μs) of 10 μM GDSP reacted with the various

calcium salts (Figure 2.3b), in comparison with the control crystal (Figure 2.3a) and non-targeted

Gd-DOTA (Figure 2.3c) reacted crystals, shows specific binding of the contrast agent to HA

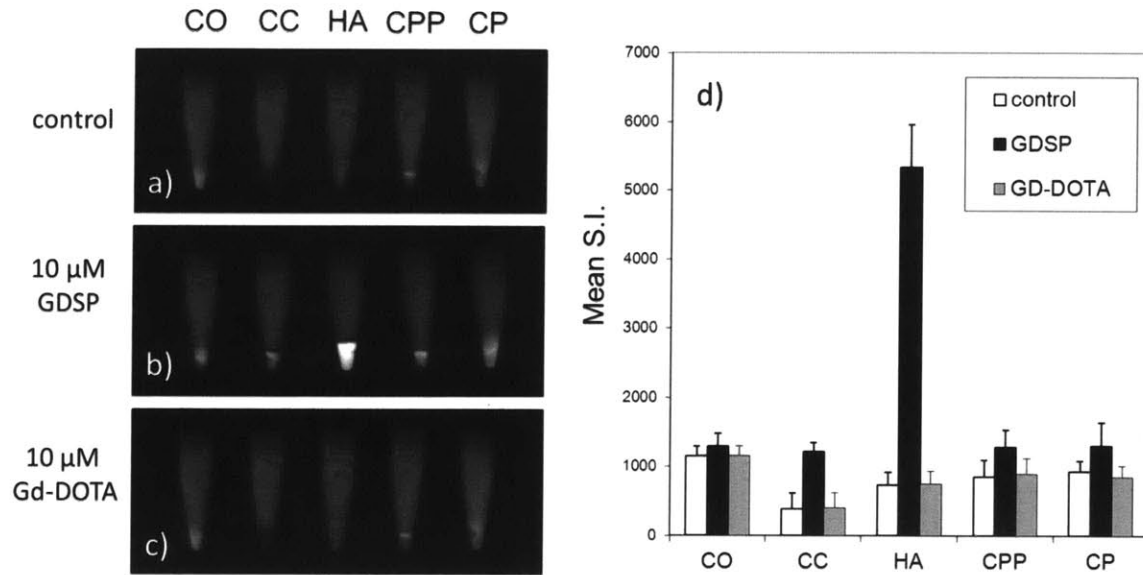relative to CO, CC, CPP and CP. The mean signal intensity over regions of interests (ROIs)

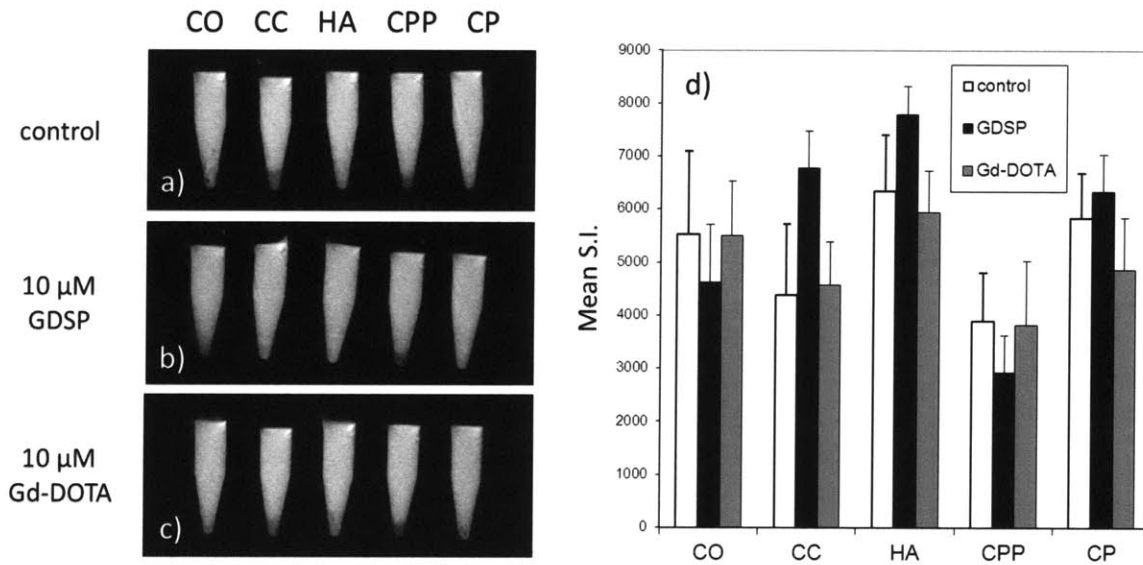Figure 2.3 – UTE MRI of contrast agent specificity

Figure 2.4 – Conventional FGRE of contrast agent specificity

outlining the crystals are compared in Figure 2.3d. The hydroxyapatite-targeted sample shows

the highest relative increase in signal intensity compared to the control crystal. GDSP binding to

HA raised mean SI by 540% whereas binding to CO, CC, CPP, and CP raised the mean SI by 10,

220, 38, and 42% respectively. The relative specificity of the contrast agent for HA compared to CO, CC, CPP, and CP was hence: 54:1, 2.5:1, 14:1, and 13:1 respectively. Comparative FGRE images (Figure 2.4a-d) show that the different crystal type cannot be distinguished by conventional imaging.

2.2.2. Sensitivity

MR images of incremental contrast agent concentrations reacted with HA were acquired to assess the contrast agent sensitivity. The HA-adsorbed contrast agent can be detected at reaction concentrations as low as 1 µM by UTE imaging with TR = 100 ms and TE = 100 µs (Figure 2.5a). At low TR the crystals cannot be seen, and at high TR the signals from both the crystals and the water become saturated. Longitudinal relaxation measurements were performed by
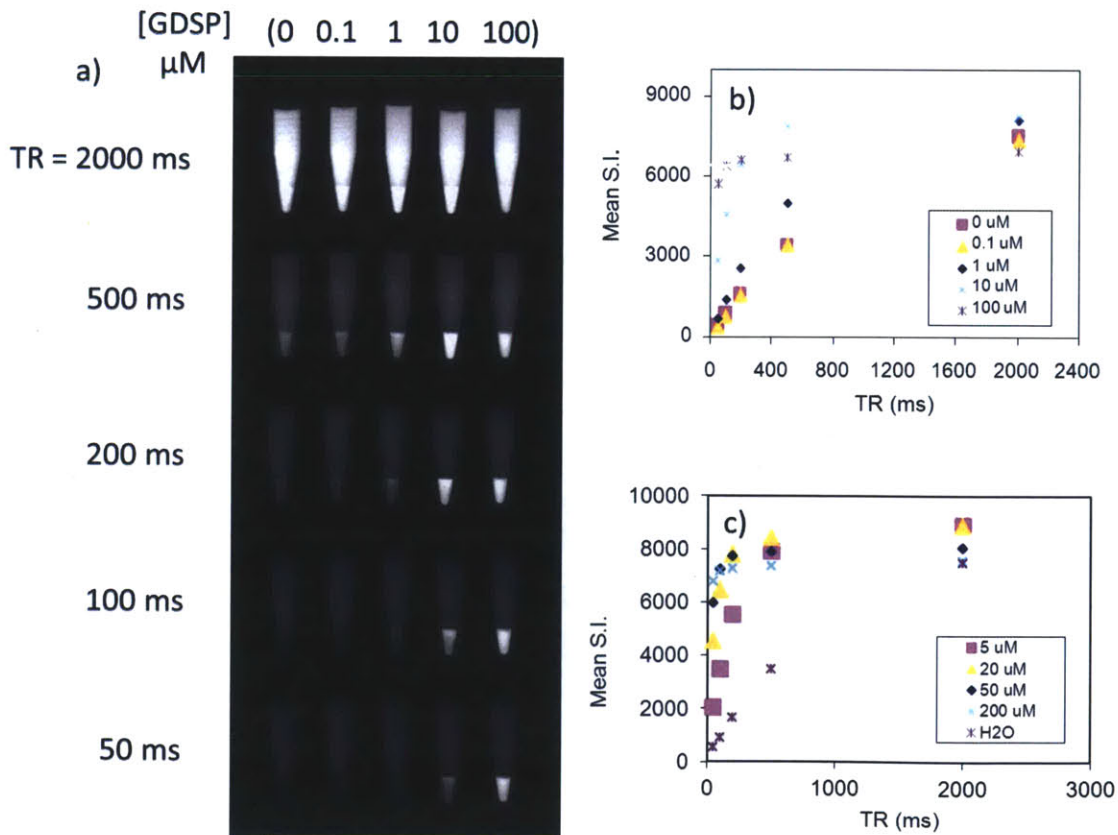

Figure 2.5 – Targeted contrast agent sensitivity

Table 2.1 – Fitted longitudinal relaxation times

[GDSP] (µM)	0	0.1	1	5	10	20	50	100	200
T_1 (ms)	932	782	475	201	100	70.4	36.2	23.3	20

imaging over increasing TR: mean ROI signal intensity for each concentration is plotted versus

time in Figure 2.5b,c. The signal equation was fit to the mean ROI signal intensities to estimate

the longitudinal relaxation times (T_1) for each reaction concentration (Table 2.1). Faster

relaxation occurs with increasing contrast agent concentration. The free unbound contrast agent,

in comparison to the bound targeted agent sensitivity of 1 µM, requires concentrations > 20 µM

for detection (Figure 2.6a). Longitudinal relaxation curves fitting the mean ROI signal intensity

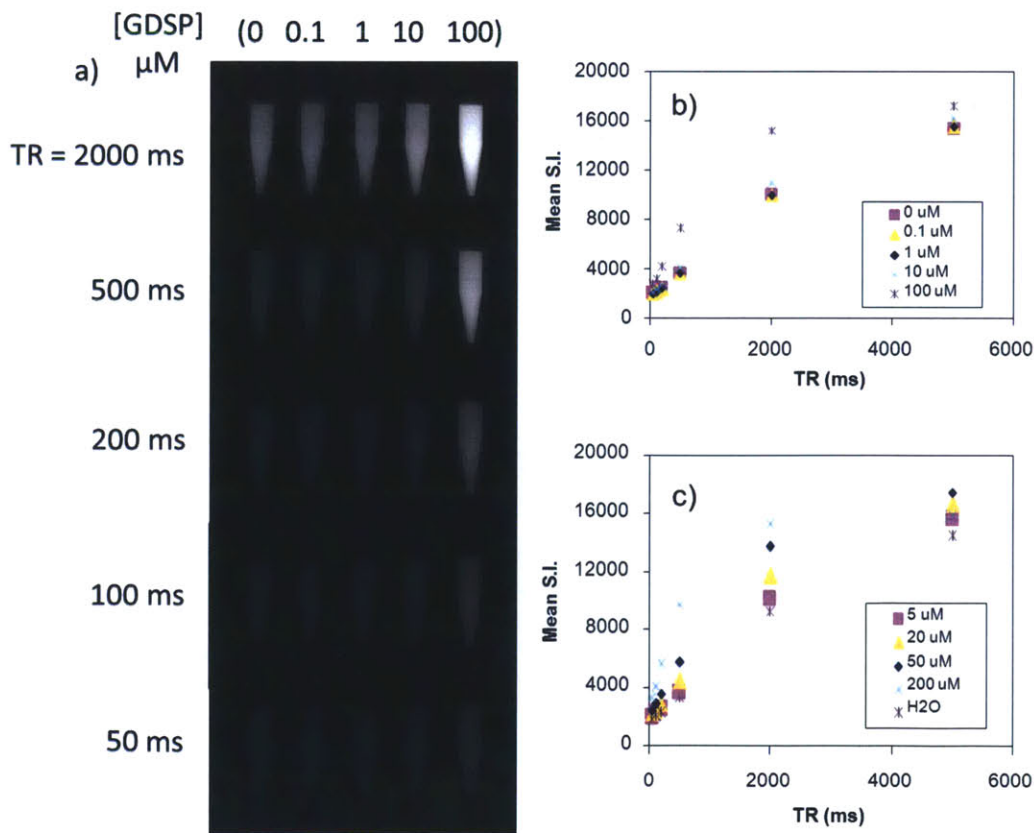over TR for varied free agent concentrations are plotted in Figure 2.6b,c.

Figure 2.6 – Free agent sensitivity

2.2.3. Free and bound agent relaxivity

The relaxivity of the free unbound contrast agent (r_1^f) was obtained by linear regression of the relaxation rate over increasing contrast agent concentration (Figure 2.7a). The slope of the fit to Eqn. 2.4 estimated the free agent relaxivity to be: $r_1^f = 5.4$ s^{-1}/mM. For the HA-targeted contrast agent, relaxation rates at high contrast agent reaction concentrations increase to a plateau (Figure 2.7b). The T_1 of the HA reacted with 1 μM GDSP was 475 ms, whereas the T_1 of the baseline HA is 945 ms. The observed apparent relaxivity of the targeted contrast agent, expressed relative to the initial reaction contrast agent concentration, was calculated by $r_1^b = \Delta R1/[GDSP]$ to be approximately 1030 s-1/mM. The apparent relaxivity of the targeted contrast agent is enhanced by over 100-fold compared to the free agent.
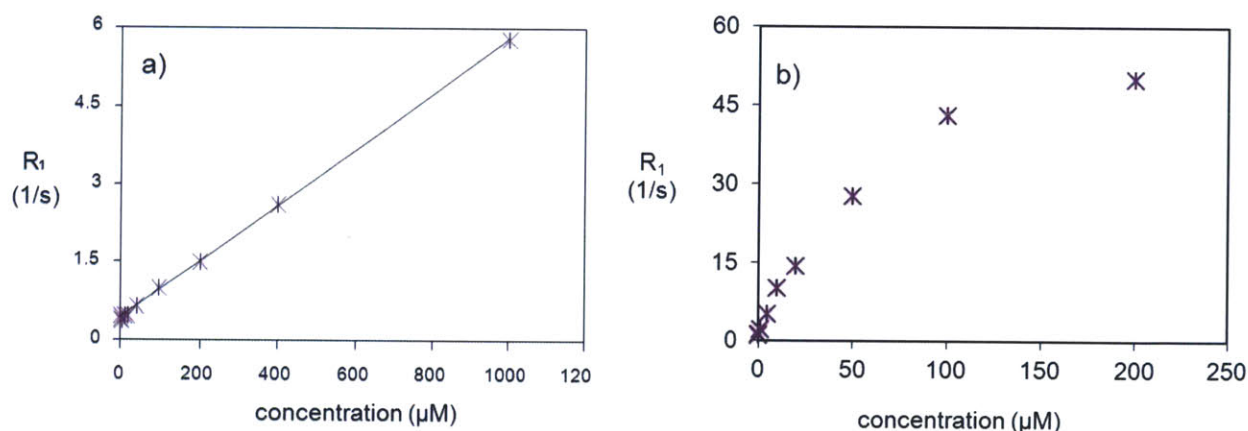

Figure 2.7 – Relaxivity of the free and targeted contrast agent

2.3. Discussion

UTE MR images of the contrast agent reacted with hydroxyapatite (HA), calcium oxalate (CO), calcium carbonate (CC), calcium phosphate (CP), and calcium pyrophosphate (CPP) were collected to assess binding specificity. The images of the control salts with no contrast agent showed that the baseline signal for each crystal type varies. The arrangement of water molecules

around the different crystal surface structures explains the different baseline signals in the control crystals. Non-targeted Gd-DOTA reacted with the calcium salts did not enhance the MR signal demonstrating that the pamidronate ligand is required for binding. The relative specificity of the contrast agent for HA over CO was high, providing increased image contrast in the malignant calcification form compared to its benign counterpart. The other calcium crystal types are not found in breast cancer calcification pathologies. Ultra-short echo time MRI, compared to conventional FGRE imaging, is necessary for image contrast of the agent binding to hydroxyapatite.

The HA-targeted contrast agent could be detected by UTE with initial reaction concentrations as low as 1 micromolar. There are a finite number of binding sites covering the HA crystal surface, and hence the amount of targeted GDSP is saturated at high concentrations. This is consistent with surface chemoadsorption according to a Langmuir isotherm, previously shown by radiolabeled HA-targeted Tb-DOTA-PAM conjugates [29]. The estimated free agent relaxivity is consistent with that of conventional small molecule non-targeted gadolinium-chelates, typically around 5 s^{-1}/mM [19]. The apparent bound contrast agent relaxivity is enhanced over one-hundred fold relative to the unbound agent and existing small molecule gadolinium contrast agents. The relaxivity enhancement may be caused by restricted rotational motion of the contrast agent when adsorbed to HA. The bound contrast agent rigidity is likely due to a combination of high-affinity chemoadsorption of pamidronate to the HA crystal surface and the short ligand-to-agent linker length [19]. The HA-targeted contrast agent used with UTE MRI enables the detection of micromolar concentration currently undetectable with conventional relaxivity contrast agents.

Relaxation described by the classical SBM theory assumes that the paramagnetic agent undergoes isotropic motion in solution and is modeled by averaging random perturbations from locally fluctuating dipole-dipole fields. Longer correlation times (slower rotating molecules) are predicted to result in higher relaxivities. The HA-targeted contrast agent, however, is rotationally restricted when bound to the crystal surface. The relaxivity of the solid surface bound contrast agent with restricted motion is not explained by current relaxation theory.

Strategies which lengthen rotational correlation times upon binding to macromolecules (e.g. to human serum albumin) have displayed relaxivities up to 80 s^{-1}/mM [21]. More recently, Gd-chelates tethered to carbon nanotube walls [30] have shown exceptionally high relaxivities, greater than 170 s^{-1}/mM. This high relaxivity was not corroborated by existing relaxivity theories, and may be explained by restriction of the contrast agent to a surface. Surface-targeted contrast agents that are rotationally inhibited may exhibit a new regime of high relaxivity with potential applications in molecular MRI.

Chapter 3. *In-vivo* MRI of hydroxyapatite calcifications

Imaging of the contrast agent binding to hydroxyapatite *in-vivo* following systemic delivery is demonstrated in this chapter. Two animal models are used to assess the contrast agent. First, the *in-vivo* specificity of the contrast agent is evaluated by MRI following systemic uptake in mice with bilateral subcutaneous implants of HA and CO slurries. Second, the application to breast cancer screening is examined by uptake imaging in female rats with breast cancer tumors expressing hydroxyapatite microcalcifications. Pre-and post-contrast MR images are compared to CT imaging to validate that UTE MRI can detect the hydroxyapatite-targeted contrast agent *in-vivo*. All of the animal experiments were IACUC approved.

3.1. Methods and materials

3.1.1. Systemic uptake to slurry implants

Subcutaneous hydroxyapatite and calcium oxalate crystal slurry implants were used to mimic malignant and benign calcification *in-vivo*. Pre- and post- contrast UTE MRI was performed to assess whether systemic delivery of contrast agent to the crystal implants can be detected in a sample size of N = 4 mice with statistical significance. The relative binding specificity (of contrast agent toward HA and CO) is estimated and the UTE images are validated by CT.

3.1.1.1. Slurry implantation: 50 mg of HA and CO, each suspended in 150 μL saline, were implanted bilaterally by subcutaneous injection (16G needle) over the right and left flanks of nude mice anaesthetized with 2.5% isoflurane/O_2 balance. The implants were injected one day prior to imaging such that the natural migration and packing of the crystals settled.

3.1.1.2. Pre- and post-contrast imaging: Pre-contrast MRI was acquired before systemic injection (retro-orbital) of the targeted contrast agent (0.13 mmol/kg). After a 4 hour uptake period, post-contrast MRI was acquired. In both of the pre-contrast and post-contrast MRI sessions, axial images were acquired by: *i*) Fast spin-echo imaging (FSE) to localize the slurries (slice thickness = 5 mm, FOV = 9 cm, matrix = 512×512, NEX = 1, TE = 2.1 ms, TR = 5000 ms); *ii*) Dual-echo UTE imaging at long and short TE (slice thickness = 5 mm, FOV = 9 cm, matrix = 256×199, NEX = 2, α = 90°, TE = 100/20000 μs, TR = 200 ms); and, *iii*) Fast gradient echo imaging (FGRE) as a conventional standard (slice thickness = 5 mm, FOV = 9 cm, matrix = 256×256, NEX = 1, α = 30°, TE = 2.1 ms, TR = 200 ms). The total MR imaging time for this protocol remains less than 15 minutes. The mice were anaesthetized with 2.5% isoflurane/O_2 balance for all imaging sessions and contrast agent injections, and were awakened for the uptake durations.

3.1.1.3. CT validation: Localization of the calcium crystals and their contrast uptake was validated using a NanoSPECT/CT (Bioscan) scanner. Continuous helical micro-CT images were collected to locate the crystal implants. Registration of the CT and MR was performed using an MR/CT visible fiducial marker to validate that the MRI UTE pre- and post-contrast images show signal enhancements in targeted crystal regions.

3.1.1.4. Image analysis: Targeted uptake was assessed (ImageJ, MATLAB) by the MRI signal intensities (SI) in the crystal regions. Dual-echo UTE subtraction images (short-long echo) were processed to reveal signal enhancement from bound contrast. The pre- and post-contrast images (FSE, UTE, UTE subtraction, and FGRE) were compared slice-by-slice to localize the crystal implants with enhanced SI. The relative change in mean ROI signal intensities from

before and after contrast injection over regions of amplified signal in each crystal type were used to estimate the relative binding specificity of the contrast agent to HA and CO *in-vivo*.

3.1.2. Systemic uptake to hydroxyapatite calcification in a breast cancer model

Towards the clinical application of screening for malignant breast cancer, MRI of targeted-contrast uptake was demonstrated in rat tumors expressing hydroxyapatite calcifications. Pre- and post- contrast UTE MRI was performed to assess whether systemic delivery of contrast agent to the calcifications shows significant signal enhancements in N = 2 rats. The UTE images were validated by CT.

3.1.2.1. Breast cancer microcalcification model: Breast cancer tumors with hydroxyapatite

calcifications were grown following the model by Liu et al. [31] (Figure 3.1a). Fischer 344 female rats were inoculated with R3230 cancer cells and administered systemic delivery of BMP-2. Calcification growth coincided with tumor necrosis, after approximately two to three weeks of tumor growth. CT was performed to monitor the tumors for calcifications before attempting MRI contrast uptake.

3.1.2.2. Pre- and post-contrast imaging: The protocol for imaging the tumor calcifications

is outlined in Figure 3.1b. Pre-contrast MRI was acquired before systemic tail vein injection of the targeted contrast agent (0.13 mmol/kg). After uptake periods of 1-4 hrs, post-contrast MRI was acquired. In both the pre-contrast and post-contrast MRI sessions, axial images were acquired by FSE (to localize the tumor), UTE (using short and long echo), and FGRE (as convention), following the protocols in 3.1.1.2. Follow-up CT was performed to validate the locations of the tumor calcifications and contrast agent uptake.
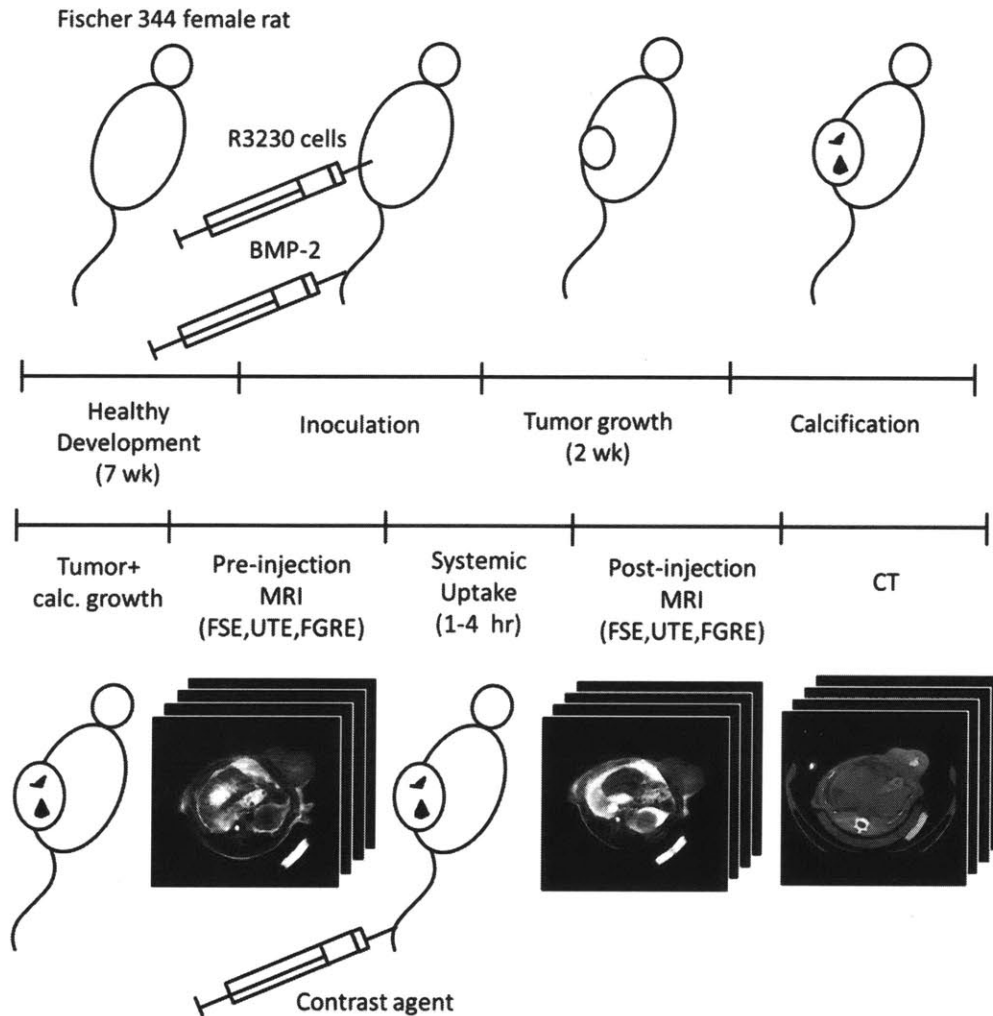
b Figure 3.1 – Animal model and *in-vivo* imaging protocol

3.1.2.3. Image analysis: Targeted uptake was assessed (ImageJ, MATLAB) by the MRI signal intensities (SI) in the tumor calcifications. The pre- and post-contrast images (FSE, UTE, UTE subtraction, and FGRE) were compared slice-by-slice to localize calcifications with enhanced SI. The relative change in mean ROI signal intensities, from before and after contrast injection, of calcified regions with amplified signal were used to estimate the effect size on signal change at the injected dose. Statistical significance of SI enhancement due to targeted

contrast was tested by comparing to the SI in non-targeted tissues. Comparative ROIs were drawn for the fiducial marker, the tumor background (excluding calcification), and muscle.

3.1.3. Statistics

The mean signal intensity enhancement, from pre- and post-contrast imaging, was compared between hydroxyapatite and calcium oxalate in the slurry implant model using a one-tailed t-test (N = 4). In the tumor calcification model, mean signal intensity enhancement was compared between hydroxyapatite and each of the fiducial, tumor background, and muscle, again using a one-tailed t-test (N = 2). Statistical significance of the t-value was assessed using $p = 0.05$.

3.2. Results

3.2.1. Hydroxyapatite and calcium oxalate slurry imaging

UTE subtraction images (short-long echoes, $TE_1=100$ μs – $TE_2=20$ ms) in Figure 3.2 demonstrate targeted contrast in the mouse crystal implants following systemic administration of the contrast agent. The pre-contrast image (Figure 3.2a) shows the baseline signal intensities for HA (dashed arrow) and CO (solid arrow). In the post-contrast image (4 hr uptake), the HA slurry implant is illuminated where contrast agent has bound to the crystals (Figure 3.2b). The CO crystal also intensifies, but to a lesser degree. Figure 3.2c shows that CT detects the HA and CO crystals with equal signal intensity, making them indistinguishable. Across the N=4 mice, the mean SI of an ROI over the crystals show a significantly greater enhancement in HA (30%) than in CO (7%): hence, the *in-vivo* relative specificity for HA over CO is 4.3-fold (Figure 3.2d).
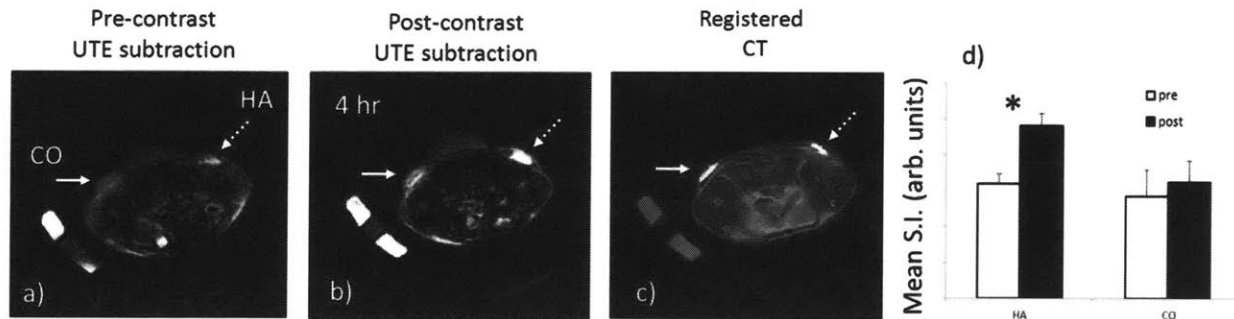
Figure 3.2 – In-vivo uptake to hydroxyapatite and calcium oxalate slurry implants

3.2.2. MRI of hydroxyapatite calcification in breast tumors

Figure 3.3 shows the pre- and post-contrast MRI in the rat tumor model. The calcifications

cannot be detected in the conventional FGRE images (Figure 3.3a,e), which are also confounded

by breathing artifact. Comparing the pre-and post-UTE images at short TE = 100 µs (Figure

3.3b,f), there is a vague illumination in the center of the tumor, but the contrast is not sufficient

to reveal the exact calcification location. In the UTE images at long TE = 20 ms (Figure 3.3c,g)

the overall signal intensity is reduced due to the decay of transverse relaxation. The short-T_2

tumor calcification becomes a dark spot at a long echo-time. Signal enhancement of the

calcification becomes apparent in the UTE subtraction images (Figure 3.3d,h). Subtracting the

long TE (low calcification signal) image from the short TE (high calcification signal) image

results in contrast that illuminates the hydroxyapatite-targeted tumor calcification.

Targeted contrast agent uptake to tumor calcifications is demonstrated in Figure 3.4. The pre-

contrast UTE subtraction images show a signal void in the calcified region of the tumor for one

animal (Figure 3.4a), and have varied signal in the second animal (Figure 3.4d). In the post-

contrast images, the signal intensity of the calcified region is amplified by the bound contrast

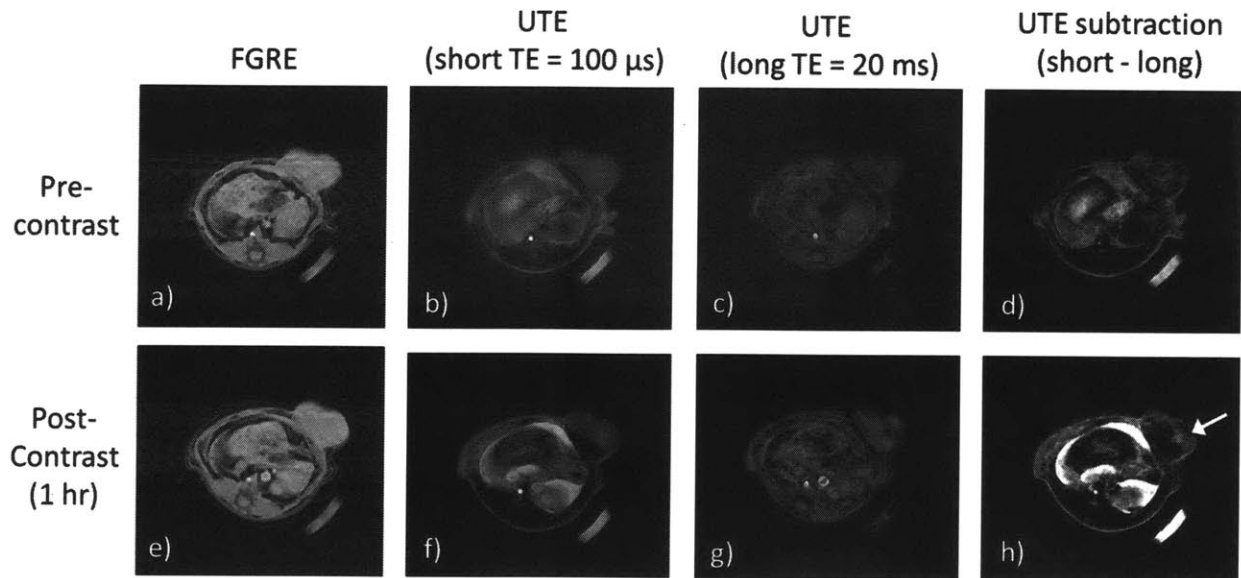agent: the targeted dose produced a SI enhancement greater than 200% in the calcified region for

Figure 3.3 – Dual-echo UTE subtraction for imaging calcifications
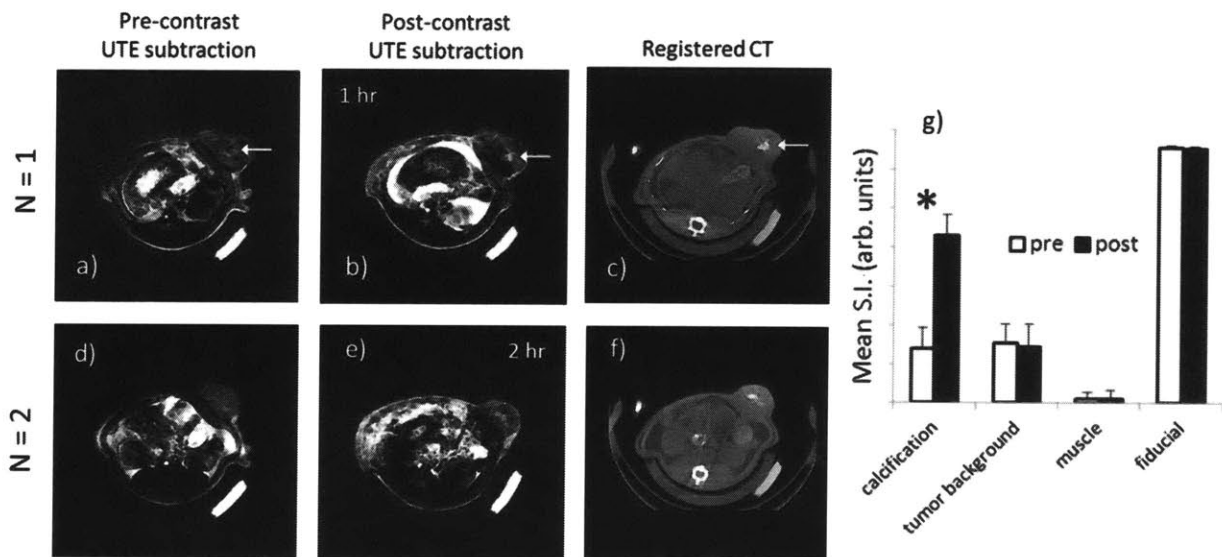

Figure 3.4 – In-vivo MRI of contrast uptake to tumor calcifications

both animals (Figure 3.4b,e). The registered CT images validate the location and morphology of the tumor calcifications (Figure 3.4c,f). The round calcification in the first animal and the crescent-shaped calcification in the second animal were both detected by dual echo subtraction UTE using the targeted contrast agent. The relative signal enhancement between pre- and post-

contrast imaging was significantly higher in the tumor calcifications than in the demarcated comparative regions (Figure 3.4g).

3.3. Discussion

Dual-echo subtraction UTE MRI is able to detect signal enhancements in hydroxyapatite calcifications targeted by systemic contrast agent delivery. Pre- and post-contrast images showed relative contrast agent specificity for hydroxyapatite over calcium oxalate in crystal slurry implants. Imaging of contrast agent uptake to hydroxyapatite calcifications was demonstrated in an animal model. Conventional MRI techniques were not able to detect the short-T_2 calcifications even with the bound contrast agent because of the decay in transverse relaxation. Furthermore, UTE required subtraction between short and long echo images to detect contrast in the hydroxyapatite-targeted calcifications. Bright signal in other areas of the UTE subtraction images, possibly originating from longer-T_2 species, may be nulled in future by dual-inversion preparation techniques [32]. Tumor calcifications could be detected reliably by UTE MRI, and their appearance closely resembled their form in comparative CT images. X-ray mammography, while well-able to detect these same calcifications, cannot distinguish whether they are made of hydroxyapatite.

The ability to distinguish hydroxyapatite from calcium oxalate calcifications could enable earlier delineation of malignant and benign breast tumors. Early identification of calcification type may reduce unnecessary biopsies and improve the positive predictive value of an initial diagnostic imaging exam [33]. In addition, early recognition of hydroxyapatite depositions may improve therapeutic management by indicating surgical removal of primary tumors before metastatic invasion. Women at high-risk of invasive breast cancer are currently being screened by DCE

MRI in which vascular contrast agents are used to assess tumor activity, but microcalcifications remain unseen using extant techniques. Thus, using an HA-targeted gadolinium contrast agent for UTE MRI in combination with DCE-MRI to detect and differentiate microcalcifications may improve clinical screening for malignant breast cancer. Ultimately, the targeted contrast agent may extend clinical applications for UTE of hydroxyapatite calcifications in other diseased tissues.

Chapter 4. Conclusions

4.1. Major contributions and impact

A gadolinium contrast agent for MRI that specifically targets hydroxyapatite and exhibits enhanced relaxivity when bound was developed. The contrast agent was specific for hydroxyapatite relative to calcium oxalate, the forms of malignant and benign breast tumor calcifications. UTE imaging was sensitive to detection of the contrast agent at reaction concentrations as low as 1 micromolar. The relaxivity of the free contrast agent was 5.4 s^{-1}/mM, comparable to that of conventional non-targeted gadolinium chelates. The apparent relaxivity of the targeted contrast agent was observed to be > 1000 s^{-1}/mM, relative to initial dose concentration. The relaxivity of the hydroxyapatite-bound contrast was enhanced relative to the free contrast agent in solution by more than two orders of magnitude due to restricted rotational motion on a solid surface. The high-relaxivity targeted contrast agent holds promise for clinical MRI of hydroxyapatite calcifications in malignant breast tumors and other calcified tissues.

The HA-targeted contrast agent was detected by UTE MRI following systemic delivery *in-vivo*. Dual-echo subtraction images were required to obtain sufficient image contrast to see targeted calcifications. Contrast delivery to subcutaneous HA and CO crystal implants in mice showed that there was a 4.3-fold specificity towards HA over CO. Pre- and post-contrast MRI of hydroxyapatite calcifications in a rat model of breast cancer detected delivery of the contrast agent throughout the entire calcified region with SI enhancements greater than 200%. The potential to distinguish HA microcalcifications by UTE using a targeted contrast agent may improve breast cancer screening by combined x-ray mammography and MRI.

4.2. Limitations and pitfalls

The characterization of relaxivity proposed in this thesis is limited to an apparent relaxivity measurement relative to dose concentration. The true relaxivity of the surface-targeted contrast agent requires knowledge of the bound agent concentration. Langmuir isotherm models relating bound and initial agent concentration could be used to determine the true relaxivity. Furthermore, classical SBM models of relaxivity assume isotropic rotation of a paramagnetic center in solution. Since the hydroxyapatite-targeted contrast agent undergoes surface chemoadsorption, it is likely to be rotationally restricted. There is no existing theory that can corroborate relaxivity on a solid surface. The theoretical extension describing relaxivity of surface restricted contrast agents is beyond the scope of this work. Nonetheless, the apparent relaxivity measurements offer a reasonable estimation of the effect that the initial delivered contrast agent concentration has on longitudinal relaxation rate.

Systemic delivery to subcutaneous slurries is a mock model for assessing the calcification specificity. Although the slurry implants and subcutaneous blood supply differ from calcifications in a vascularized tumor, there is still uptake of the contrast agent to the crystals. The breast cancer calcifications represent a better delivery model, but lack a CO control for benign tumors. The rat model used is the only current animal model available for expressing breast cancer calcifications. In human breast conditions, calcifications up to 2 mm may be regarded as suspicious, but those that are any larger are representative of benign pathologies [34]. Cancerous breast tumors typically have calcifications measuring under 0.5 mm. Microcalcifications seen in clinical x-ray mammography are very small compared to the spatial resolution of conventional MR imaging. Emerging techniques for higher-resolution MRI of

solids [35] combined with the high relaxivity of the contrast may provide detectable sub-voxel signals sufficient for imaging hydroxyapatite microcalcifications in breast cancer.

4.3. Future work and recommendations

Dose response and tumor monitoring experiments of the contrast agent would demonstrate two limits: the lowest injectable contrast agent concentration that can be detected in calcifications, and the smallest detectable calcification size. Minimizing the required contrast agent dose may avoid possible toxicity complications from a gadolinium-chelate being indefinitely bound *in-vivo*. Further assessment of biodistribution, clearance, and toxicity will support the translation of the hydroxyapatite-targeted contrast agent toward clinical human imaging. The ability to detect sub-millimeter microcalcifications will ensure that the technique is suitable for imaging breast tumors. Ultimately, the contrast agent could be used for UTE in conjunction with DCE-MRI. The vascular uptake would be imaged in the minutes after injection, and the calcification targeting would be imaged hours afterward. In clinical application, UTE MRI of the hydroxyapatite-targeted contrast agent could distinguish calcifications in malignant breast tumors, reducing unnecessary biopsies and affording earlier diagnosis and treatment.

Bibliography

[1] Breast cancer facts and figures 2011-2012. American Cancer Society. 2011.

[2] Smith RA, Cokkinides V, Brooks D, Saslow D, Shah M, Brawley OW. Cancer screening in the United States, 2011: A review of current American Cancer Society guidelines and issues in cancer screening. *CA: A Cancer Journal for Clinicians*. 2011; 61(1): 8-30.

[3] Rosselli Del Turco M, Ciatto S, Bravetti P, Pacini P. The significance of mammographic calcifications in early breast cancer detection. *Radiologia Medica*. 1986; 72: 7-12.

[4] Winston JS, Yeh IT, Evers K, Friedman AK. Calcium oxalate is associated with benign breast tissue. Can we avoid biopsy? *American Journal of Clinical Pathology*. 1993; 100(5): 488-92.

[5] Morgan MP, Cooke MM, McCarthy GM. Microcalcifications associated with breast cancer: an epiphenomenon or biologically significant feature of selected tumors? *Journal of Mammary Gland Biology and Neoplasia*. 2005; 10(2): 181-7.

[6] Morgan MP, Cooke MM, Christopherson PA, Westfall PR, McCarthy GM. Calcium hydroxyapatite promotes mitogenesis and matrix metalloproteinase expression in human breast cancer cell lines. *Molecular Carcinogenesis. 2001; 32(3): 111-7.*

[7] Tse GM, Tan PH, Pang AL, Tang AP, Cheung HS. Calcification in breast lesions: pathologists' perspective. *Journal of Clinical Pathology*. 2008; 61(2): 145-51.

[8] Saslow D, Boetes C, Burke W, et al. American Cancer Society guide-lines for breast screening with MRI as an adjunct to mammography. *CA: A Cancer Journal for Clinicians*. 2007; 57(2): 75-89.

[9] Mann RM. The effectiveness of MR imaging in the assessment of invasive lobular carcinoma of the breast. *Magnetic Resonance Imaging Clinics of North America*. 2010; 18(2): 259-76.

[10] Warner E, Plewes DB, Hill KA, Causer PA, Zubovits JT, Jong RA, Cutrara MR, DeBoer G, Yaffe MJ, Messner SJ, Meschino WS, Piron CA, Narod SA. Surveillance of BRCA1 and BRCA2 mutation carriers with magnetic resonance imaging, ultrasound, mammography, and clinical breast examination. Journal of the American Medical Association. 2004; 292(11): 1317-25.

[11] Bazzocchi M, Zuiani C, Panizza P, Del Frate C, Soldano F, Isola M, Sardanelli F, Giuseppetti GM, Simonetti G, Lattanzio V, Del Maschio A. Contrast-enhanced breast MRI in patients with suspicious microcalcifications on mammography: results of a multicenter trial. *American Journal of Roentgenology*. 2006; 186(6): 1723-32.

[12] Huang W, Fisher PR, Dulaimy K, Tudorica LA, O'Hea B, Button TM. Detection of breast malignancy: diagnostic MR protocol for improved specificity. *Radiology*. 2004; 232(2): 585-91.

[13] Kneeshaw PJ, Turnbull LW, Smith A, Drew PJ. Dynamic contrast enhanced magnetic resonance imaging aids the surgical management of invasive lobular breast cancer. *European Journal of Surgical Oncology*. 2003; 29(1): 32-7.

[14] Chan CF, Keenan NG, Nielles-Vallespin S, Gatehouse P, Sheppard MN, Boyle JJ, Pennell DJ, Firmin DN. Ultra-short echo time cardiovascular magnetic resonance of atherosclerotic carotid plaque. *Journal of Cardiovascular Magnetic Resonance*. 2010 Mar 26;12:17.

[15] Robson MD, Bydder GM. Clinical ultrashort echo time imaging of bone and other connective tissues. *NMR in Biomedicine*. 2006; 19(7): 765-80.

[16] Solomon I. Relaxation processes in a system of two spins. *Physical Review*. 1955; 99(2): 559-566.

[17] Bloembergen N. Proton relaxation times in paramagnetic solutions. *The Journal of Chemical Physics*. 1957; (27): 572-573.

[18] Bloembergen N, Morgan LO. Proton relaxation times in paramagnetic solutions. Effects of electron spin relaxation. *The Journal of Chemical Physics*. 1961; (34): 842-850.

[19] Caravan P. Strategies for increasing the sensitivity of gadolinium based MRI contrast agents. *Chemical Society Reviews*. 2006; 35: 512-523.

[20] Avedano S, Tei L, Lombardi A, Giovenzana GB, Aime S, Longo D, Botta M. Maximizing the relaxivity of HSA-bound gadolinium complexes by simultaneous optimization of rotation and water exchange. *Chemical Communications*. 2007; (45): 4726-8.

[21] Caravan P. Protein-targeted gadolinium-based magnetic resonance imaging (MRI) contrast agents: design and mechanism of action. *Accounts of Chemical Research*. 2009; 42(7): 851-62.

[22] Jarvis MF, Burns CJ, Pauls HW, Assal A, Kim JS, Cheney DL, Youssefyeh RD. Characterization of the bisphosphonate recognition site on hydroxyapatite using radioligand binding techniques with [14C] citric acid. *Calcified Tissue International*. 1993; 52(5): 372-77.

[23] Mukherjee S, Huang C, Guerra F, Wang K, Oldfield E. Thermodynamics of bisphosphonates binding to human bone: a two-site model. *Journal of the American Chemical Society*. 2009; 131(24): 8374–8375.

[24] Guénin E, Monteil M, Bouchemal N, Prangé T, Lecouvey M. Syntheses of phosphonic esters of alendronate, pamidronate and neridronate. *European Journal of Organic Chemistry*. 2007; 20: 3380- 91.

[25] Humblet V, Misra P, Frangioni JV. An HPLC/mass spectroscopy platform for the development of multimodality contrast agents and targeted therapeutics: prostate-specific membrane antigen small molecule derivatives. *Contrast Media in Molecular Imaging*. 2006; 1(5): 196-211.

[26] Bhushan KR, Misra P, Liu F, Mathur S, Lenkinski RE, Frangioni JV. Detection of breast cancer microcalcifications using a dual-modality SPECT/NIR fluorescent probe. *Journal of the American Chemical Society*. 2008; 130(52):17648-9.

[27] Lenkinski RE, Ahmed M, Zaheer A, Frangioni JV, Goldberg SN. Near-infrared fluorescence imaging of microcalcification in an animal model of breast cancer. *Academic Radiology*. 2003; 10(10): 1159-64.

[28] Bhushan KR, Tanaka E, Frangioni JV. Synthesis of conjugatable bisphosphonates for molecular imaging of large animals. *Angewandte Chemie International Edition*. 2007; 46(42): 7969-71.

[29] Vitha T, Kubíek V, Hermann P, Kolar ZI, Wolterbeek HT, Peters JA, Lukeš I. Complexes of DOTA−bisphosphonate conjugates: probes for determination of adsorption capacity and affinity constants of hydroxyapatite. *Langmuir*. 2008; 24(5): 1952-58.

[30] Sitharaman B, Kissell KR, Hartman KB, Tran LA, Baikalov A, Rusakova I, Sun Y, Khant HA, Ludtke SJ, Chiu W, Laus S, Toth E, Helm L, Merbach AE, and Wilson LJ. Superparamagnetic gadonanotubes are high-performance MRI contrast agents. *Chemical Communications*. 2005; 3915-3917.

[31] Liu F, Bloch N, Bhushan KR, De Grand AM, Tanaka E, Solazzo S, Mertyna PM, Goldberg N, Frangioni JV, Lenkinski RE. Humoral bone morphogenetic protein 2 is sufficient for inducing breast cancer microcalcification. *Molecular Imaging*. 2008; 7(4): 175-86.

[32] Du J, Takahashi AM, Bae WC, Chung CB, Bydder GM. Dual inversion recovery, ultrashort echo time (DIR UTE) imaging: creating high contrast for short-T(2) species. *Magnetic Resonance in Medicine*. 2010; 63(2): 447-55.

[33] Lazarus E, Mainiero MB, Schepps B, Koelliker SL, Livingston LS. BI-RADS lexicon for US and mammography: interobserver variability and positive predictive value. Radiology. 2006; 239(2): 385-91.

[34] Kopans DB. Breast Imaging. *Lippincott Williams & Wilkins*. 2007.

[35] Frey MA, Michaud M, VanHouten JN, Insogna KL, Madri JA, Barrett SE. Phosphorus-31 of hard and soft solids using quadratic echo line narrowing. *Proceedings of the National Acadamy of Science*. 2012; 109(14): 5190-5195.

Appendix 1.

A.1. Characterization of pamidronate and contrast agent syntheses

The molecular weights of the methyl-protected pamidronate, the final contrast agent, and the contrast agent synthesis intermediates were validated by LC-MS using a Waters (Milford, MA, USA) HPLC pump equipped with a SymmetryC18 reverse-phase HPLC column. The column eluate was divided using a flow splitter (Upchurch Scientific, Oak Harbor, WA, USA) into an evaporative light scattering detector (ELSD, Sedere, Olivet, France) and a Waters Micromass LCT TOF-ES mass spectrometer. For mass spectrometry in positive mode, the mobile phase was solvent A = H_2O + 0.1% formic acid, and the stationary phase was solvent B = acetonitrile + 0.1% formic acid. For mass spectrometry in negative mode, the mobile phase was solvent A = 10 mM TEAA in H_2O, and the stationary phase was solvent B = absolute MeOH. Capillary voltage was –3317V, sample cone voltage was –50V, and the flow rate was 0.6 mL/min. The LC-MS ion mode and gradient conditions for characterizing the molecular weights for each product are summarized in Table A1. ELSD detection and mass/charge ratios of corresponding peaks for each product are shown in Figures A1-A7.

Table A1 - Validation of contrast agent synthesis by LC-MS

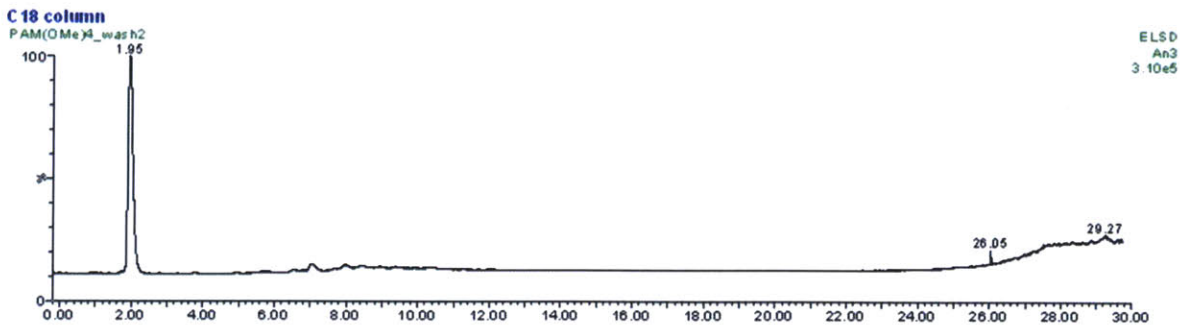| Compound	HPLC			TOF-MS		
	Time (min)	Solvent B (%)*	Retention time (min)	MW (g/mol)	Observed (m/z)	Ion Mode (+/−)
(5')	0-5; 5-30	0; 0-90	2.0	291	293	(+)
(2)	0-5; 5-30	0; 0-90	16.7	569	569	(+)
(3)	0-5; 5-30	0; 0-90	7.3	434	435	(+)
(4)	0-5; 5-30	0; 0-90	11.7	989	989	(+)
(5)	0-5; 5-30	0; 0-90	12.4	765	766	(+)
(6)	0-5; 5-30	0; 0-90	13.6	919	921	(+)
(7)	0-5; 5-30	0; 0-40	11.6	862	859	(−)
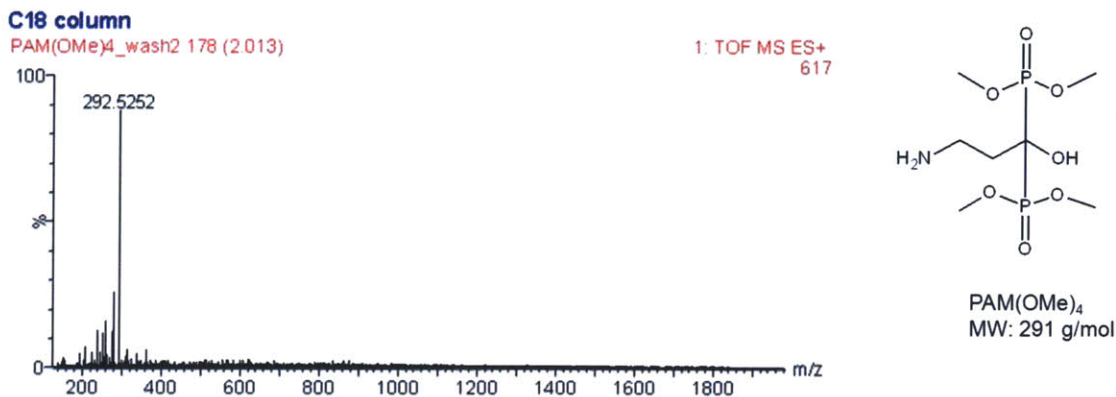
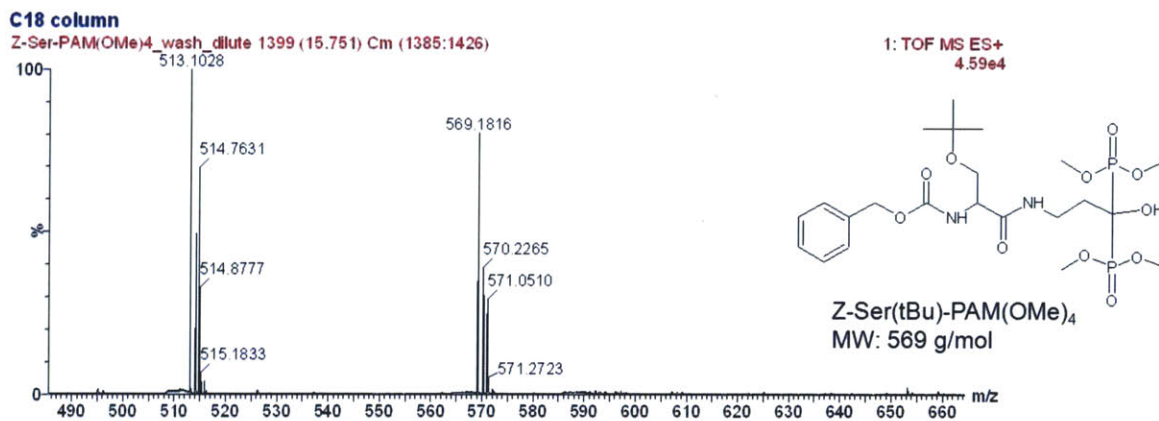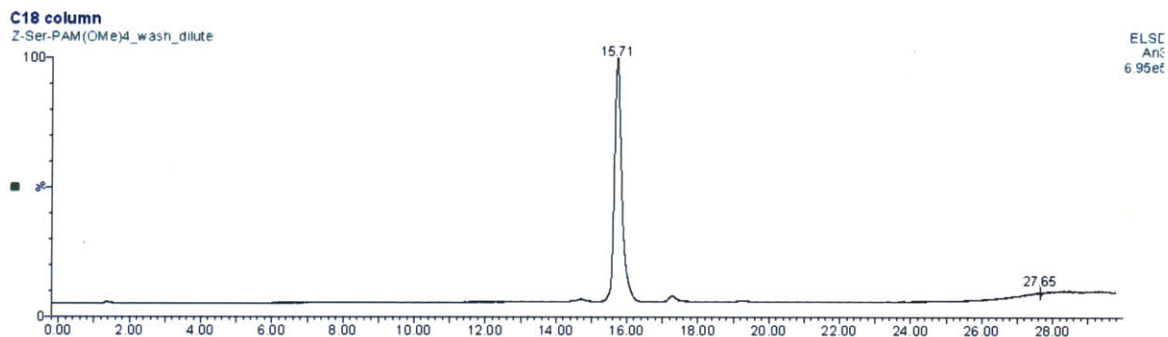Figure A1 – LC/MS characterization of (5) *PAM(OMe)₄*

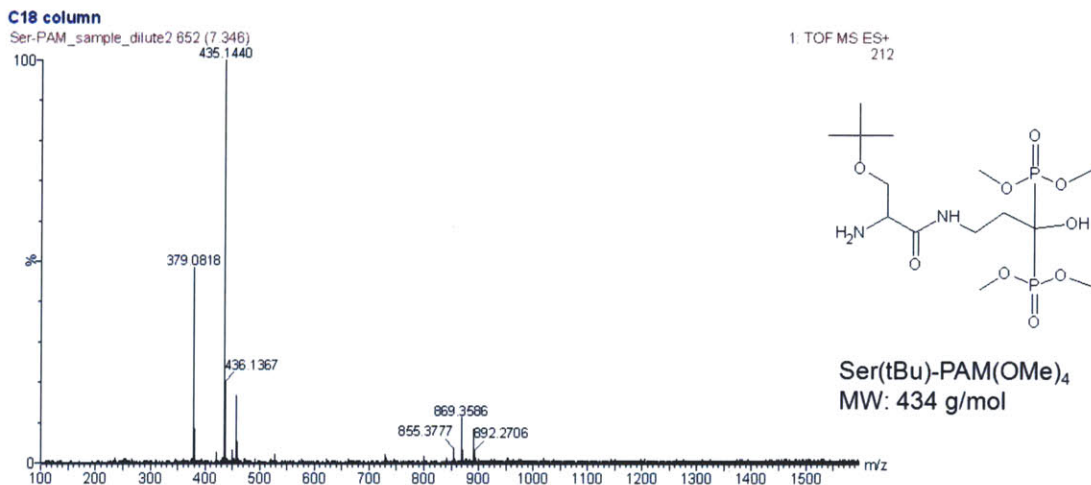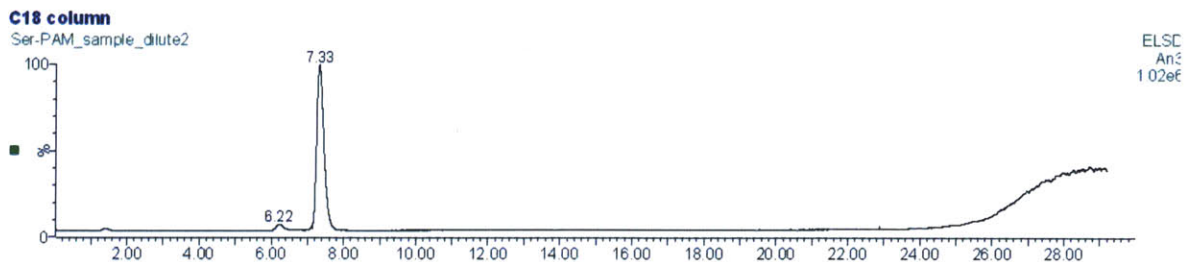Figure A2 – LC/MS characterization of (7) *Z-Ser(tBu)-PAM(OMe)₄*

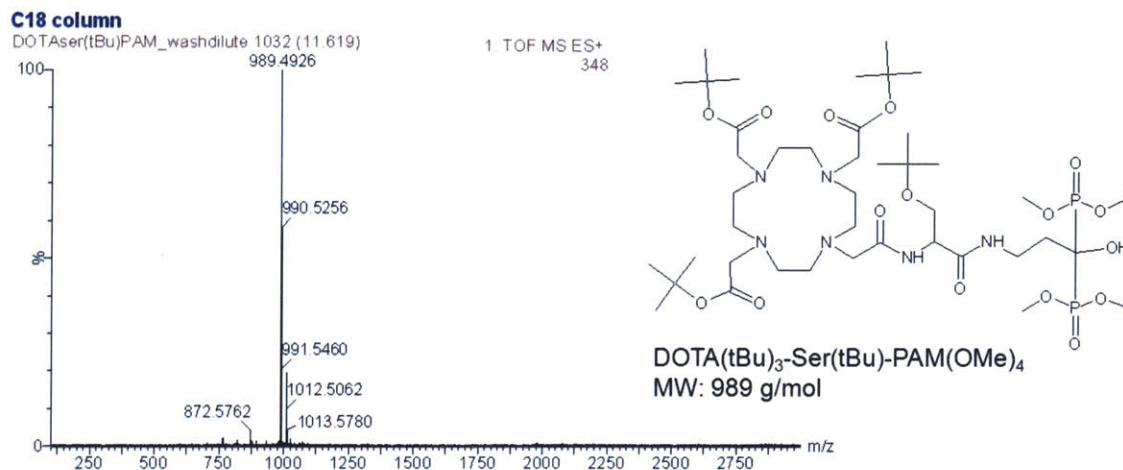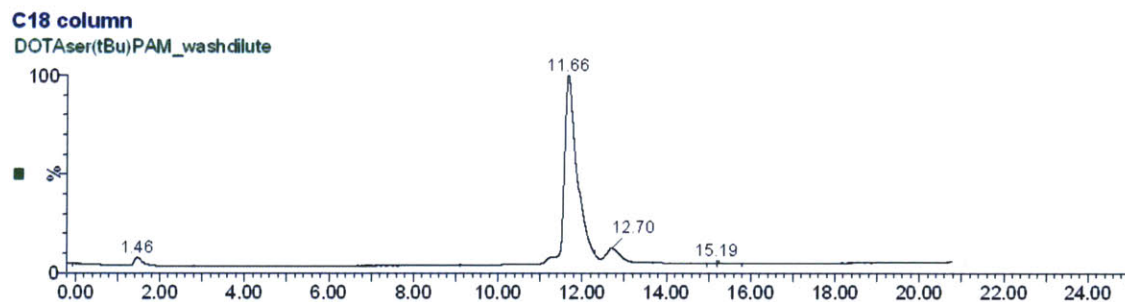Figure A3 – LC/MS characterization of (8) *Ser(tBu)-PAM(OMe)₄*

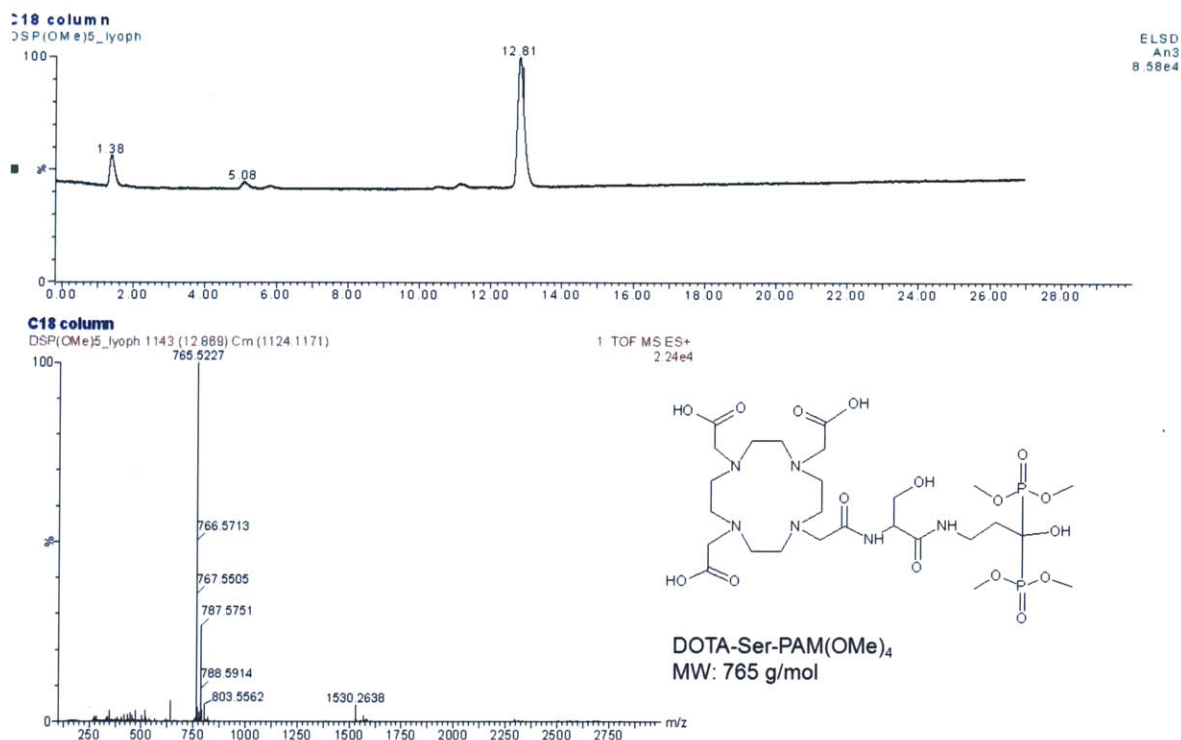Figure A4 – LC/MS characterization of (9) *DOTA(tBu)₃-Ser(tBu)-PAM(OMe)₄*

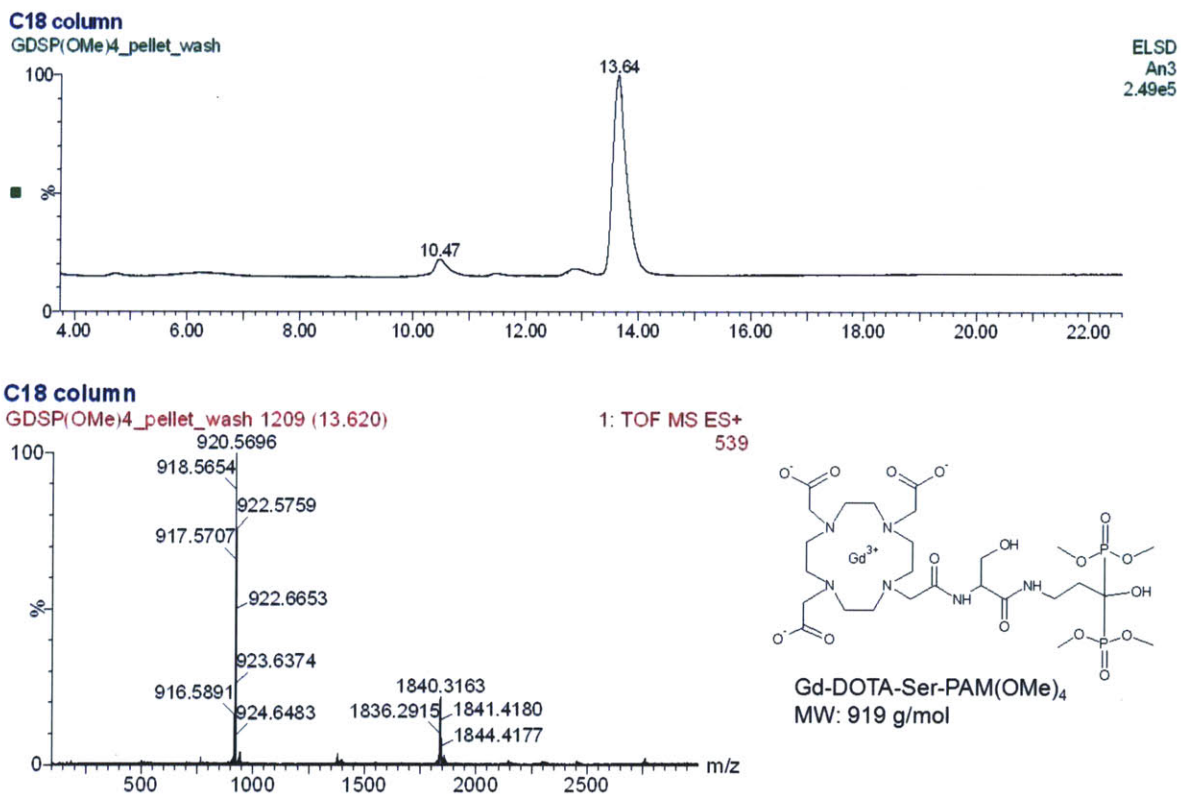Figure A5 – LC/MS characterization of (10) *DOTA-Ser-PAM(OMe)₄*

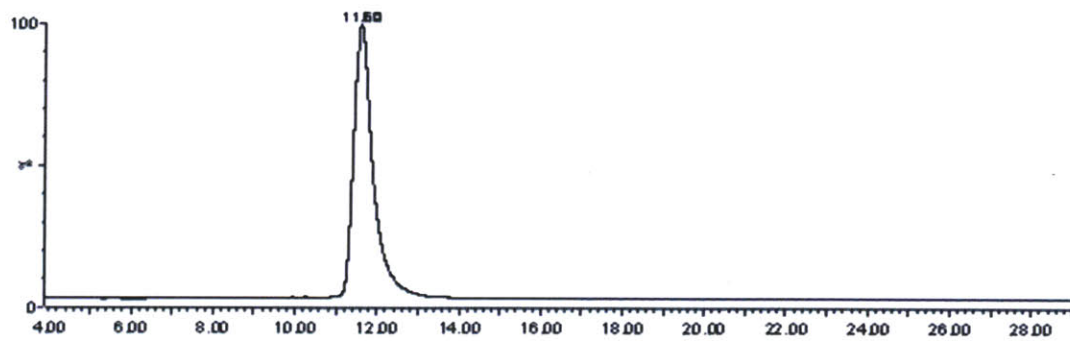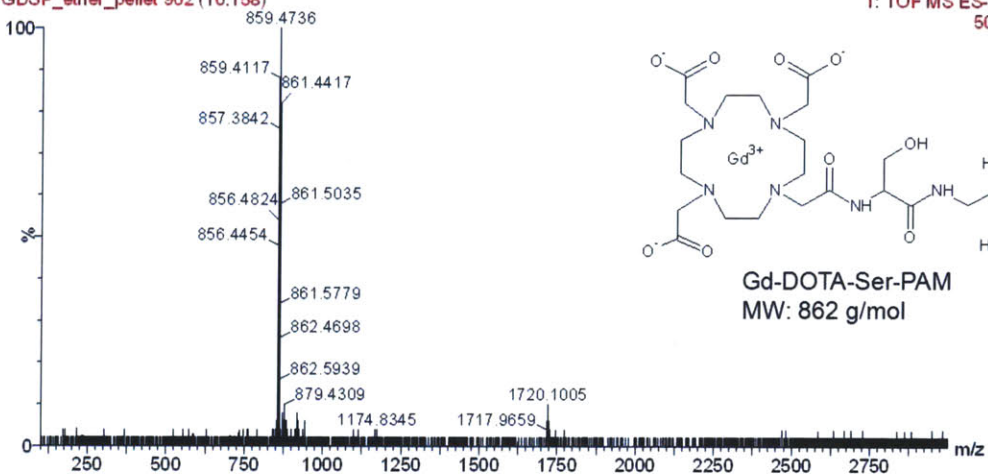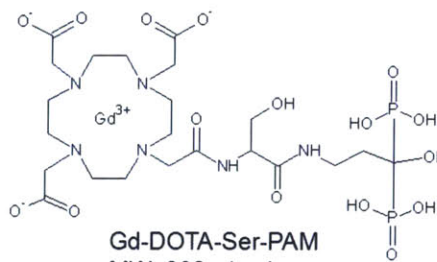Figure A6 – LC/MS characterization of (11) *Gd-DOTA-Ser-PAM(OMe)₄*

Figure A7 – LC/MS characterization of (12) *Gd-DOTA-Ser-PAM*

Vita

Name: Jonathan Marmurek

Home: Guelph, Ontario, Canada

Previous education: The University of Western Ontario
                               MESc Biomedical Engineering
                               BESc Electrical Engineering

Related publications and patents:

Marmurek J, Lunsford E, Nasr K, Vinogradov E, Liu F, Madhuranthakam AJ, Frangioni JF, Lenkinski RE. *A hydroxyapatite-targeted gadolinium contrast agent for MRI of breast cancer microcalcifications.* Proceedings of the 20th Annual Scientific Meeting of the International Society of Magnetic Resonance in Medicine: 2012; 1640.

Marmurek J, Nasr K, Vinogradov E, Madhuranthakam AJ, Frangioni JF, Lenkinski RE. *Enhanced-relaxivity of hydroxyapatite-targeted gadolinium contrast agents.* Proceedings of the 19th Annual Scientific Meeting of the International Society of Magnetic Resonance in Medicine: 2011; 457.

Marcus CM, **Marmurek J**, Aptekar JW, Von Maltzahn G. *Telemetry through remote detection of nmr-active particles.* US Patent Application 12/812,069: filed Jan. 9, 2009.